

***RXTE* Studies of X-ray Spectral Variations with Accretion Rate in 4U 1915-05**

P. F. Bloser, J. E. Grindlay

*Harvard-Smithsonian Center for Astrophysics,
60 Garden Street, Cambridge, MA 02138
pbloser@cfa.harvard.edu*

pbloser@cfa.harvard.edu

and

D. Barret, L. Boirin

*Centre d'Etude Spatiale des Rayonnements, CNRS/UPS,
9 Avenue du Colonel Roche, 31028 Toulouse Cedex 04, France
Didier.Barret@cesr.fr*

ABSTRACT

We present the results of detailed spectral studies of the ultra-compact low mass X-ray binary (LMXB) 4U 1915-05 carried out with the *Rossi X-ray Timing Explorer* (*RXTE*) during 1996. 4U 1915-05 is an X-ray burster (XRB) known to exhibit a ~ 199 -day modulation in its 2–12 keV flux. Observations were performed with the PCA and HEXTE instruments on *RXTE* at roughly one-month intervals to sample this long-term period and study accretion rate-related spectral changes. We obtain good fits with a model consisting of a blackbody and an exponentially cut-off power law. The spectral parameters are strongly correlated with both the broad-band (2–50 keV) luminosity and the position in the color-color diagram, with the source moving from a low hard state to a high soft state as the accretion rate increases. The blackbody component appears to drive the spectral evolution. Our results are consistent with a geometry in which the soft component arises from an optically thick boundary layer and the hard component from an extended Comptonizing corona. Comparing our results with those of a similar study of the brighter source 4U 1820-30 (Bloser et al. 2000), we find that the two ultra-compact LMXBs occupy similar spectral states even though the transitions occur at very different total luminosities.

Subject headings: accretion, accretion disks — stars: individual (4U 1915-05) — stars:neutron
— X-rays:stars

1. Introduction

Recent advances in broad-band X-ray astronomy observations have led to rapid progress in the study of Low Mass X-ray Binaries (LMXBs) containing low-magnetic field neutron stars (NSs). Many of these systems exhibit bright X-ray bursts at low accretion rates; those that do are known as X-ray bursters (XRBs). Narrow-band observations at high energies by BATSE and SIGMA have shown that XRBs can emit hard X-rays at ~ 100 keV (Barret & Vedrenne 1994, Tavani & Barret 1997 and references therein). The lack of simultaneous low energy observations has until recently made it difficult to relate the hard X-ray emission to the softer blackbody and disk blackbody components long known to exist in XRBs and other NS systems (e.g. Mitsuda et al. 1984). The broad-band spectral sensitivities of the *Rossi X-ray Timing Explorer* (*RXTE*, Bradt, Rothschild, & Swank 1993) and *BeppoSAX* (Boella et al. 1997) have now allowed detailed modeling of the complete X-ray to hard X-ray (1–200 keV) spectra of several XRBs with a variety of complex physical models including blackbody, disk blackbody, power law, Comptonization, reflection, and line components (e.g., Church et al. 1998; Guainazzi et al. 1998; in 't Zand et al. 1999; Olive et al. 1999, Piraino et al. 1999a; Piraino et al. 1999b; Barret et al. 1999, 2000; Bloser et al. 2000). These observations promise to reveal the relationship between the hard and soft spectral components, the geometry of the emitting regions, and the dependence of each on the mass accretion rate.

In this paper we present the spectral results of *RXTE* observations of a particularly interesting XRB, the 50-minute binary 4U 1915-05. This system is well-known as the first dipping source discovered (White & Swank 1982; Walter et al. 1982), and was the first XRB to show clear evidence for a binary nature (Walter et al. 1982). The source has generated extensive interest due to the fact that its dip period, ~ 50 minutes, is close to but significantly shorter than the period of modulation of its optical counterpart, a $m_V \sim 21$ blue star (Grindlay et al. 1988; Callanan et al. 1995). This has led to numerous interpretations, including the possibility that the system is a hierarchical triple (Grindlay et al. 1988). From evolutionary calculations on low-mass systems with short orbital periods, Nelson, Rappaport & Joss (1986) find that the companion is likely a hydrogen-deficient star that is neither fully degenerate nor burning helium. Smale et al. (1988) argue that the lack of X-ray eclipses, combined with the orbital parameters expected for such a companion star, constrain the orbital inclination to be $< 79^\circ$. From analysis of an X-ray burst that showed photospheric radius expansion, Yoshida (1993) derived a distance for 4U 1915-05 of 9.3 kpc. A long-term X-ray modulation with a rough period of 199 days is also seen in *Vela 5B* data (Priedhorsky & Terrell 1984a), indicating a long-term modulation in the accretion rate.

The goal of the present investigation is to observe the broad-band spectrum of the persistent (non-burst and non-dip) emission from 4U 1915-05 with the PCA and HEXTE instruments on *RXTE* in order to study the relationships between spectral parameters and accretion rate. (Analysis of these same data for the 50-minute X-ray dip period and related periodic behavior is presented by Chou, Bloser, & Grindlay 2000.) The 199-day variation in the flux from 4U 1915-05 is similar to that in another compact XRB, 4U 1820-30, which has a 176-day period (Priedhorsky & Terrell 1984b). 4U 1820-30 only exhibits X-ray bursts in the lowest state, indicating that the modulation

is due to accretion rate variations and not, for example, to disk precession effects. Although 4U 1915-05 is a dimmer source and thus able to emit X-ray bursts over a wider range of its luminosity, this similarity implies that the 199-day modulation is also due to accretion rate variations. Thus these two sources provide good laboratories for the study of accretion-related spectral changes. We have observed 4U 1915-05 at roughly monthly intervals over the course of a year to sample this 199-day period. (A re-analysis of the *Vela 5B* data by Smale & Lochner (1992) puts the significance of this period at only $\sim 80\%$; however, the source may still be counted on to vary its luminosity on this rough timescale.) A similar analysis of 4U 1820-30 has been presented by Bloser et al. (2000).

2. Previous Spectral Observations of 4U 1915-05

Previous spectral observations of 4U 1915-05 have been performed by a variety of experiments. In early work, simple, one-component models were fit to the spectra. White & Swank (1982) fit a power law (PL) with photon index $\alpha = 1.6$ – 1.7 to *OSO-8* data and a thermal bremsstrahlung model with $kT = 12$ keV to (non-simultaneous) *Einstein* MPC+SSS data. The *Einstein* luminosity was 1.2 – $1.5 \times 10^{37} (D/10\text{kpc})^2$ ergs s^{-1} (0.5–60 keV). Smale et al. (1988) fit *EXOSAT* data with a PL with $\alpha = 1.8$ and found a luminosity of $7.6 \times 10^{36} (D/10\text{kpc})^2$ ergs s^{-1} (0.1–15 keV). Extensive observations were performed by *Ginga* (Yoshida 1993), which obtained data over a wide range of source luminosities. These spectra could be fit by a combination of a cut-off power law (CPL; an approximation of Comptonization) and a broad gaussian at 7 keV. Using the *Ginga* results of Yoshida (1993), Barret et al. (1996) defined three distinct intensity/spectral states for 4U 1915-05 with typical values of the power law index α , exponential cut-off energy E_c , and 1–37 keV luminosity L : a high/very soft state ($\alpha = 1.0$, $E_c \sim 8$ – 10 keV, $L = 1.2 \times 10^{37}$ ergs s^{-1}); an intermediate/hard state ($\alpha = 1.7$, $E_c \gtrsim 50$ keV, $L = 6$ – 7×10^{36} ergs s^{-1}); and a low/soft state ($\alpha = 1.5$, $E_c \sim 25$ keV, $L = 3 \times 10^{36}$ ergs s^{-1}). Barret et al. (1996) note that the evidence for softening at low luminosity is marginal and needs to be confirmed.

Two high-energy experiments on *CGRO* failed to detect 4U 1915-05 above 50 keV. Bloser et al. (1996) analyzed four years of BATSE data and report a 2σ upper limit of 6.3×10^{36} ergs s^{-1} on the 20–100 keV luminosity of the source for 10 day integrations. Barret et al. (1996) did not detect 4U 1915-05 in a pointed OSSE observation, reporting 2σ upper limits in two energy bands of 1.7×10^{35} ergs s^{-1} (50–98 keV) and 1.3×10^{35} ergs s^{-1} (98–158 keV).

More recent observations have allowed two-component models to be fit. Church et al. (1997) fit 0.7–10 keV *ASCA* data with a combination of a PL and blackbody (BB), finding a best-fit blackbody temperature $kT_{BB} = 2.14$ keV and $\alpha = 2.42$. (Note however that Ko et al. (1999) are able to fit the same data with a single power law with $\alpha \sim 1.75$; the blackbody of Church et al. 1997 shares flux with the power law near 10 keV, and so their power law is steeper.) Morley et al. (1999) use the same model on *ROSAT* data (0.1–2 keV) and find $kT_{BB} = 1.95$ keV and $\alpha = 2.32$. Finally, the first true hard X-ray detection of 4U 1915-05 was reported by Church et al. (1998), who detect the source above 100 keV in a broad-band (0.1–100 keV) *BeppoSAX* observation. They

fit a combination of a CPL and BB and find $kT_{BB} = 1.62$ keV, $\alpha = 1.61$, and $E_c = 80 \pm 10$ keV.

A brief summary of previously-reported spectral results on 4U 1915-05 is presented in Table 1.

3. Observations and Analysis

3.1. *RXTE* Observations and Data Reduction

The PCA instrument on *RXTE* is made up of five Xenon proportional counter units (PCUs, numbered 0–4) sensitive from 2–60 keV with a total area of about 6500 cm² (Bradt, Rothschild, & Swank 1993). The HEXTE instrument consists of two clusters of four NaI(Tl)/CsI(Na) phoswich scintillation detectors sensitive from 15–200 keV with an effective area of 1600 cm²; these clusters rock on and off source to obtain background measurements (Rothschild et al. 1998). The ASM is comprised of three Scanning Shadow Cameras (SSCs) with one-dimensional slit masks and 6° × 90° fields of view that monitor the fluxes of bright X-ray sources several times a day in the 2–12 keV band (Levine et al. 1996).

Nine joint PCA/HEXTE pointed observations of 4U 1915-05 were performed at roughly monthly intervals between 1996 February 10 and 1996 October 29. An additional ten observations were performed on consecutive days between 1996 May 14 and 23. A complete log of the observations is given by Boirin et al. (2000). The *RXTE*/ASM 2–12 keV light curve of 4U 1915-05 during this period is shown in Figure 1, with the times of our pointed observations marked. Each point represents the one-day average of the ASM count rate. Although the 199-day period reported by Priedhorsky & Terrell (1984a) is not obvious in Figure 1, in agreement with the findings of Smale & Lochner (1992), it is clear that we have observed the source in a variety of intensity states ranging from ~ 0.2 –2 ASM counts s⁻¹, or ~ 2.7 –27 mCrab.

The data were divided into 70 segments (typical length ~ 1200 seconds) of persistent emission, excluding bursts and dips, and reduced using the standard *RXTE* analysis tools contained in FTOOLS 4.2. For the HEXTE spectral analysis we used standard archive mode data and extracted spectra with *saextract* v4.0b. Deadtime corrections were computed using *hxtdead* v0.0.1. For our color-color diagram and PCA spectral analysis we used the “Standard 2” data, which provide 128 energy channels between 2 and 100 keV with 16-second time resolution. Spectra were extracted with *saextract*, and the v2.2.1 response matrices (January 1998) were used.

Complications arose in the analysis of the PCA data from the fact that the PCA gain was lowered twice during 1996. Our first two observations, performed on 1996 February 10 and March 13, occurred during PCA Gain Epoch 1, while the remaining observations occurred during Gain Epoch 3. Different background models and response matrices are needed for each Gain Epoch. During both Epoch 1 observations the source was “bright” (defined as having a count rate greater than 40 cts s⁻¹ PCU⁻¹), and so we used the “new sky-VLE” (August 1999) models recommended for Epoch 1 to generate a background using *pcabackest* v2.1b. We found that the background for

the March 13 observation was computed correctly, but that the February 10 background was badly overestimated. We attempted to correct the February 10 background by renormalizing the activation component, as recommended by the Guest Observer Facility web pages. When producing the color-color diagram (see Section 3.2), however, we found that the points from these data segments were badly misplaced. We therefore excluded the February 10 data from further analysis. The Epoch 3 backgrounds were computed using *pcabackest* with the appropriate Epoch 3 bright and faint source background models, depending on the source count rate (see Table 1 in Boirin et al. (2000)).

In this paper we present a spectral analysis of the persistent emission. A timing analysis of the persistent emission and bursts, including the discovery of twin kilohertz quasi-periodic oscillations (QPOs), is given by Boirin et al. (2000). An analysis of the X-ray dip period and optical period is given by Chou, Bloser, & Grindlay (2000), and a study of the spectral evolution in dipping will be the subject of a forthcoming paper.

3.2. Color-Color Diagram and Parameterization of Accretion Rate

A color-color diagram (CCD) was produced from the PCA data with one point for each of the 70 data segments. Only PCUs 0, 1, and 2 were on continuously during all observations, and so only data from these PCUs are included here. The soft and hard colors are defined as the ratios of background-subtracted PCA count rates in the bands 3.5–6.4 keV and 2.0–3.5 keV, and 9.7–16.0 keV and 6.4–9.7 keV, respectively. Data from Gain Epoch 1 (the 1996 March 13 observation) are difficult to include in the same diagram because the channel-to-energy conversion is different, leading to differences in the energy band channel boundaries. We have attempted to divide the March 13 counts into the proper energy bands by employing fractional channel boundaries and assigning the correct fraction of counts in the “in-between” channels to either the higher or lower band based on the fitted spectral shape. The CCD is shown in Figure 2. We observe 4U 1915-05 in the lower and upper banana branches, two of the states associated with “atoll” sources (Hasinger & van der Klis 1989). Although it appears in Figure 2 that the points with the highest hard color form a separated cluster, suggesting that 4U 1915-05 enters the island state as well, the timing analysis shows that the source never exhibits the high frequency noise typically observed in atoll sources in the island state (Boirin et al. 2000). We shall refer to the lowest state in our data as the “*RXTE* low state,” and note that it refers not to the island state but the lower banana branch. The Epoch 1 data segments are indicated by the open squares. As these data represent the source at its brightest, we expect them to lie in the upper banana portion of the CCD, and indeed this is where they appear. Due to the background and gain uncertainties mentioned above, however, their exact position should be treated with caution.

It is generally believed that in atoll sources the mass accretion rate \dot{M} increases monotonically as the source moves from the island state, through the lower banana, and into the upper banana branch (Hasinger & van der Klis 1989). Méndez et al. (1999) defined the parameter S_a to measure

the position of an atoll source within its CCD and thus parameterize its accretion rate. We follow Méndez et al. (1999; see also Bloser et al. 2000) and approximate the shape of the CCD track with a spline, as shown in Figure 2. S_a is then defined as the distance along this curve, as measured from the *RXTE* low state. Thus we may use S_a in addition to the source luminosity to study accretion rate-related changes in spectral parameters. We have not used the suspect Epoch 1 data points in generating the S_a track. In order to use S_a as the basis of comparison for all of our data, we have assigned values of S_a to the Epoch 1 points according to the ratio of their total luminosity to luminosities of the Epoch 3 data.

3.3. Spectral Fitting

For our spectral analysis data segments were grouped according to their position in the CCD. Spectra were first extracted for each of the 70 data segments. These spectra were then grouped into eleven equal bins in S_a and combined together, with an average value of S_a and the total exposure time computed for each bin. Thus we had a total of eleven spectra to fit (see Table 2).

The spectral analysis was performed using XSPEC v10.0 (Arnaud 1996). Spectra for each PCU and HEXTE cluster were reduced separately and combined within XSPEC. Due to systematic uncertainties in the response matrices, only HEXTE data above 20 keV were used. Based on fits to archival Crab data (Bloser et al. 2000; see also Sobczak et al. 1999; Barret et al. 2000; Wilms et al. 1999) we use only PCA data between 2.5 and 20.0 keV from PCUs 0 & 1. (Although PCU 4 also gives good fits for Crab data, it was rarely on during our 4U 1915-05 observations.) We note that Epoch 1 Crab data gave larger systematic deviations in the residuals than Epoch 3 data, especially below 5–6 keV. The relative normalizations of the two PCUs and two HEXTE clusters were left as free parameters, since there still exist large uncertainties in the relative flux normalizations; all spectral model normalizations reported here are obtained from PCU 0. A systematic error of 1% was added to all PCA channels using *grppha*. In Figure 3 we show two representative PCA and HEXTE spectra of 4U 1915-05, one from the *RXTE* low state and one from the high state. The hardening of the spectrum at low luminosity is clear. In the *RXTE* low state the source is detected by HEXTE only up to 50 keV, as opposed to the high energy detection by *BeppoSAX* (Church et al. 1998).

All spectra were initially fit with the two-component model used by Church et al. (1998) for the *BeppoSAX* data consisting of a cut-off power law plus a blackbody (CPL + BB). This model provided a good fit to all eleven spectra, and in all cases the inclusion of the BB improved the fit greatly over the CPL alone. In addition, the residuals of the fit to the brightest spectrum (1996 March 13) showed an excess near 6 keV which could be fit with a gaussian line at $6.14_{-1.07}^{+0.18}$ keV with $\sigma = 0.23_{-0.23}^{+1.91}$ keV. Including this gaussian improved the fit significantly ($> 99.9\%$ significance from an F-test), and the line energy is roughly consistent with that of a neutral Fe $K\alpha$ line, though the parameters are highly uncertain. We note that the March 13 data are from Epoch 1, and so effects in the residuals near 5–6 keV should be treated with caution. In Figure 4 we show two examples

of spectra from PCUs 0 and 1 and HEXTE clusters A and B fit with the CPL + BB model. These are the same two spectra shown in Figure 3; now we show the raw counts with the folded model, the residuals, and the unfolded spectra with each component plotted separately. The gaussian is included in the March 13 spectrum.

Additional models were fit to the data as well. The spectra of several XRBs have recently been fit with detailed Comptonization models (Barret et al. 1999; Barret et al. 2000; Guainazzi et al. 1998; Piraino et al. 1999a; Piraino et al. 1999b; Bloser et al. 2000). We therefore fit our 4U 1915-05 spectra with the recently-developed Comptonization model of Titarchuk (1994), called the *CompTT* model in XSPEC. The parameters of interest are the temperature kT_e and optical depth τ of the Comptonizing electron cloud, and the temperature of the cool seed photons kT_W , assumed to follow a Wien law. Good fits were found to all but the dimmest three observations with a combination of this model and a blackbody (CompTT + BB). In the case of the dimmest observations no cutoff could be determined, and so the electron temperature kT_e could not be constrained. Both the CPL and CompTT models were also tried with the blackbody component replaced by a multi-color disk blackbody (DBB; Mitsuda et al. 1984). Here the parameters are the color temperature of the inner disk kT_{in} and the projected inner disk radius $R_{in}\sqrt{\cos\theta}$, where θ is the inclination of the system. Physically realistic fits could only be found with this model for the brightest six observations.

The insensitivity of the PCA below 2 keV did not allow us to determine the hydrogen column density N_H from our spectral fits. It was therefore necessary to freeze N_H at previously-determined values for all spectra. The values of N_H found from previous X-ray observations are listed in Table 1. The hydrogen column density measured from the galactic H I survey of Stark et al. (1992) is $N_H = 1.96 \times 10^{21} \text{ cm}^{-2}$ (Smale et al. 1988; preliminary Stark results reported as private communication). Based on these numbers, which are all in reasonable agreement, we took a rough average and set $N_H = 2.0 \times 10^{21} \text{ cm}^{-2}$ and kept it frozen for all our spectral fits.

4. Results

The best-fit spectral parameters for the CPL + BB model are given in Table 2 with the average value of S_a for all included data. The parameters for the CompTT + BB model are given in Table 3 for the eight spectra for which they could be derived. In Table 2 we include the total integration time for each spectrum, the effective radius of the BB emitting surface R_{BB} , and the ratio L_{BB}/L_H of the BB luminosity to the hard spectral component luminosity in the 2–50 keV band covered by the PCA and HEXTE. In Table 3 we give the best-fit temperature of the seed photons kT_W , the Comptonizing y -parameter, defined as $y = 4kT_e\tau^2/m_e c^2$, and the effective Wien radius R_W of the seed photons (in 't Zand et al. 1999; Bloser et al. 2000). The fits are very good for both models for all spectra; in fact, the values of χ^2_ν are always < 1 , indicating that the systematic errors may have been over-estimated.

In Figure 5 we show the spectral parameters of the CPL + BB model as a function of S_a , and thus presumably of \dot{M} . It is immediately obvious that all parameters are strongly correlated with S_a . As S_a increases the blackbody temperature kT_{BB} increases steadily and the relative contribution of the blackbody component increases from $< 15\%$ to $\sim 30\%$. The power law photon index α decreases smoothly as S_a increases, while the cutoff energy E_c makes a rather sudden transition at $S_a \sim 1.3$ from > 100 keV to ~ 40 keV. (Note however that even the lower limits on E_c for the dimmest three spectra lie well above the highest energy, 50 keV, at which the source is detected, and so should be treated with caution.) This transition value of S_a corresponds roughly to the “vertex” at the leftmost corner of the CCD. From the behavior of the spectral parameters it is clear that 4U 1915-05, like most systems, moves from a low, hard state to a high, soft state as the accretion rate increases. Note that when fitting a CPL model it is not α but E_c that indicates the hardness of the spectrum. Note also that the BB component appears to be the dominant factor in driving the spectral evolution of the source: kT_{BB} is very strongly correlated with S_a , and the large increase in L_{BB}/L_H corresponds to the probable quenching of the Comptonizing corona indicated by the drop in E_c .

In Figure 6 we show the spectral parameters of the CompTT + BB model as a function of S_a for the brightest eight spectra. Again the parameters are correlated with S_a , though not as strongly (due partly to the absence of the three lower state spectra). There is an indication that τ increases from ~ 6 to ~ 14 and kT_e decreases from ~ 7 to ~ 4 as S_a increases, but the error bars are large. The BB parameters are similar to those in the CPL + BB model, though again with larger uncertainties. Although the derived CompTT + BB parameters are similar to those found in other sources (Barret et al. 1999; Barret et al. 2000; Guainazzi et al. 1998; Piraino et al. 1999a; Piraino et al. 1999b; Blosler et al. 2000), the smaller error bars and more robust correlations found in Figure 5 indicate that the CPL + BB model provides a better description of the 4U 1915-05 data.

Fits were also performed using CPL + DBB and CompTT + DBB models. Only the brightest six observations gave acceptable fits. The CPL and CompTT parameters were similar to those found using the CPL + BB and CompTT + BB models. The DBB parameters in both cases did not show any correlation with S_a . For the CPL + DBB model the parameters were $kT_{in} \sim 0.6$ keV and $R_{in} \sim 8$ km. For the CompTT + DBB model the parameters were $kT_{in} \sim 0.9$ keV and $R_{in} \sim 6$ km, with greater scatter and large error bars.

5. Discussion

Our *RXTE* results for the CPL + BB model may be compared to those of previous investigations. Based on the spectral parameters of the CPL + BB model shown in Figure 5, we have observed 4U 1915-05 in the intermediate/hard and high/very soft states defined by Barret et al. (1996) from the *Ginga* data (Yoshida 1993). The transition occurs at a broad-band luminosity of $\sim 7\text{--}8 \times 10^{36}$ ergs s^{-1} , consistent with the *Ginga* results. We do not see evidence for a low/soft state

in the *RXTE* data; however, our observations do not reach as low a luminosity as the *Ginga* observations. Translating our lowest luminosity value into the 1–37 keV *Ginga* band gives $\sim 6 \times 10^{36}$ ergs s^{-1} , well above the value of $\sim 3 \times 10^{36}$ ergs s^{-1} for the *Ginga* low/soft state. In addition, the *BeppoSAX* observation described by Church et al. (1998) found a well-determined cut-off energy of 80 ± 10 keV, which is excluded at the 90% confidence level for our *RXTE* low state. This could indicate spectral softening at low luminosity. Extrapolating their spectral parameters into the 2–50 keV band of *RXTE* gives a luminosity of 4.5×10^{36} ergs s^{-1} , also lower than the lowest value seen by *RXTE*. Thus we cannot rule out a low/soft state at luminosities fainter than those observed by *RXTE*. Such a low/soft state would be difficult to explain in terms of the current physical picture of XRBs.

We can extrapolate our spectral results to higher energy for comparison with the non-detections by BATSE and OSSE (Bloser et al. 1996; Barret et al. 1996). Our *RXTE* low state spectrum would give a 20–100 keV luminosity of 3.8×10^{36} ergs s^{-1} . This is consistent with the 2σ upper limit of 6.3×10^{36} ergs s^{-1} found by BATSE for the 20–100 keV band (Bloser et al. 1996). In the 50–98 keV band our *RXTE* low state spectrum gives a luminosity of 1.2×10^{36} ergs s^{-1} , which is well above the OSSE upper limit of 1.7×10^{35} ergs s^{-1} for this band. Our high state spectrum, however, gives a consistent 50–98 keV value of 4×10^{34} ergs s^{-1} . Thus our data support the conclusion of Barret et al. (1996) that 4U 1915-05 was in the high state during the OSSE observation.

One of the major issues in the interpretation of XRB spectra is the origin of the hard versus soft spectral components (e.g., White, Stella, & Parmar 1988; Guainazzi et al. 1998; Olive et al. 1999, Barret et al. 1999, 2000). While it seems clear from spectral and timing similarities with black hole systems that the hard component must arise from Comptonization in some form of hot corona (Barret et al. 2000), both the source of the cool photons that are up-scattered and the source of the soft thermal component are the subject of debate. The soft spectral component could be dominated by thermal emission from either the inner accretion disk or an optically thin boundary layer where the accreted matter hits the NS surface. (It seems likely that in reality soft emission could come from both sources, but current instruments are unable to separate the two.) Our good CPL + BB fits, which employ a single-temperature blackbody appropriate for an optically thick boundary layer, support the latter of these two pictures. The temperature kT_{BB} increases monotonically with S_a , as might be expected if the BB luminosity increases monotonically with \dot{M} , while the small derived equivalent radius R_{BB} implies that only a narrow equatorial band around the NS is emitting. Such small values of R_{BB} have been seen before in 4U 1915-05 (Church et al. 1997; Morley et al. 1999; Church et al. 1998), and in other sources as well (White, Stella, & Parmar 1988; Church et al. 1998; Bloser et al. 2000; Church and Balucińska-Church 2000). In this picture the hot corona is then supported by soft photons from the disk (hard emission powered by the boundary layer is not favored due to the similarities between NS and BH spectra). A complication is the fact that the ratio of the BB flux to the hard PL flux L_{BB}/L_H is always less than 30%. Sunyaev & Shakura (1986) showed that, if relativistic effects are taken into account, the luminosity of the boundary layer should be at least equal to that of the disk. Again, many authors have noted

a similar discrepancy in other sources (White, Stella, & Parmar 1988; Barret et al. 1999, 2000). In the case of 4U 1915-05 a possible explanation is simply that, at such a high inclination, part of the boundary layer emission is being blocked by the inner disk. The decrease in R_{BB} as S_a increases (Figure 5) may support this notion, since perhaps the inner disk can become thicker as the accretion rate increases and obscure more of the boundary layer.

In contrast, our attempts to fit the soft component with a disk blackbody model produced unconvincing results, due to the small values of the inner disk radius derived. The value of R_{in} must be adjusted for the effects of electron scattering in the inner disk according to the relation $R_{eff} = f^2 R_{in}$ where $f = 1.7$ (Ebisawa et al. 1994; Shimura & Takahara 1995; Barret et al. 2000). Assuming the maximum inclination angle of 79° (Smale et al. 1988) this gives inner disk radii of ~ 53 km for the CPL + DBB model and ~ 40 km for the CompTT + DBB model. These values are only slightly larger than the radius of the marginally stable orbit around a $1.4 M_\odot$ NS, and it seems unlikely that in a dim source like 4U 1915-05 the disk could extend this far in. In addition, the value of R_{in} shows no correlation with S_a . Boirin et al. (2000) show that the frequency of the kilohertz QPOs in 4U 1915-05 increases with S_a for all observations, which is usually interpreted in terms of the inner disk radius decreasing (e.g., Miller, Lamb, & Psaltis 1998). Thus the inner disk in 4U 1915-05 is probably moving inward as the accretion rate increases, a fact not reflected in the derived values of R_{in} . We conclude that the DBB model is not a good description of the soft component in our data. It is possible that the edge-on nature of 4U 1915-05 is making emission from the inner accretion disk difficult to detect directly.

Our data are thus more consistent with a picture in which the soft spectral component is produced by an optically thick boundary layer which is partially blocked from view by the inner disk. This soft component is the most strongly correlated with the accretion rate, as seen in Figure 5, and is therefore the component which drives the spectral changes, despite the fact that the hard component contains a larger fraction of the flux. As the temperature kT_{BB} increases, soft thermal photons quench the Compton up-scattering in the corona, and the cut-off energy E_c of the power law decreases. It appears in Figure 5 that the sharp decrease in E_c coincides roughly with an increase in the relative luminosity of the BB. This geometrical picture is supported by the work of Church et al. (1998), Morley et al. (1999), and Church et al. (1997), all of whom find that the dips in 4U 1915-05 may be modeled by a compact blackbody emitter being occulted while an extended hard X-ray emitter is only partially covered. A spectral analysis of the PCA dip data will be the subject of a future paper. We note, however, that Bloser et al. (2000) found that the soft spectral component in 4U 1820-30, a source very similar to 4U 1915-05 in many ways (though with a lower inclination), *could* be described as a DBB. In this picture the hard power law emission arises from a hot, optically thin flow *within* the inner disk radius (Barret et al. 2000; Bloser et al. 2000). Since 4U 1915-05 is a dimmer source than 4U 1820-30, at first glance it would seem to be an even better candidate to support a hot, optically thin accretion flow.

In Figure 7 we show our CPL + BB fits for 4U 1915-05 with those of Bloser et al. (2000) for 4U 1820-30, now showing spectral parameters as a function of total 2–50 keV luminosity to

allow direct comparison. The assumed distances are 9.3 kpc for 4U 1915-05 and 6.4 kpc for 4U 1820-30. It is clear that 4U 1820-30 is always a more luminous source than 4U 1915-05, and yet the behavior of the CPL component is qualitatively similar. Using E_c as an indicator, both sources move from a low, hard state to a high, soft state as the luminosity increases, and in both sources the transition happens relatively suddenly. The transition occurs at different luminosities in each source, however: $7\text{--}8 \times 10^{36}$ ergs s^{-1} in 4U 1915-05, 3×10^{37} ergs s^{-1} in 4U 1820-30. The value of E_c is higher in 4U 1915-05 than in 4U 1820-30 in equivalent states, as might be expected in a lower luminosity source, but they do not form a continuous sequence with luminosity; $E_c = 9$ keV at 1.44×10^{37} ergs s^{-1} in 4U 1915-05, but $E_c = 23$ keV at 2.31×10^{37} ergs s^{-1} in 4U 1820-30. Thus something other than total luminosity, or accretion rate, must determine when an XRB makes the transition to a low state. The behavior of the BB component does appear to form a continuous sequence with luminosity: kT_{BB} increases steadily with luminosity in 4U 1915-05 until it reaches 2.5 keV at 1.4×10^{37} ergs s^{-1} . In 4U 1820-30, the luminosity is always above 1.4×10^{37} ergs s^{-1} , and kT_{BB} is nearly constant at ~ 2.5 keV.

We note that Church and Balucińska-Church (2000) have fit a sample of LMXBs containing NS primaries with a CPL + BB model and found that, as the luminosity increases, R_{BB} increases considerably while kT_{BB} decreases slightly. Our results for 4U 1915-05 and 4U 1820-30 (Bloser et al. 2000) seem to contradict this trend, as the values of kT_{BB} are roughly the same for the sources while R_{BB} increases only very slightly for 4U 1820-30, despite a large difference in luminosity (Figure 7). The Church and Balucińska-Church (2000) sample covers a much larger range of luminosity (up to several $\times 10^{38}$ ergs s^{-1}), however, and differences between 4U 1915-05 and 4U 1820-30 could well be lost in the scatter. More compelling is the fact that each of the sources in the Church and Balucińska-Church (2000) sample were observed only once. We have followed 4U 1915-05 throughout its CCD, and kT_{BB} clearly increases with increasing accretion rate and luminosity. Again, it seems that the total luminosity of a source does not determine its state so much as its own internal variations. In addition, the Church and Balucińska-Church (2000) sources were observed only between 1–10 keV, perhaps limiting the accuracy of the spectral fits.

The differences in spectral parameters between the two sources are reflected in their CCDs. In Figure 8 we compare the CCDs of 4U 1915-05 and 4U 1820-30 (Figure 2 of Blaser et al. 2000). The S_a tracks for both sources are indicated for clarity. Although both sources cover the same range in soft color, 4U 1820-30 nearly always has a lower value of the hard color, reflecting its low values of E_c . The two CCDs overlap at the 4U 1820-30 island state, and these points fall in the same region of the CCD as do points in the fourth S_a bin of 4U 1915-05 ($S_a = 1.36$). The values of E_c at this location are indeed similar, within the errors: $31.25^{+19.16}_{-7.48}$ keV for 4U 1915-05, $23.07^{+2.91}_{-2.36}$ keV for 4U 1820-30. The 4U 1915-05 power law is harder, however ($\alpha = 1.85$ versus 2.05), and the blackbody temperature is lower ($kT_{BB} = 1.51$ keV versus 2.57 keV). The 2–50 keV luminosities are 5.3×10^{36} ergs s^{-1} for 4U 1915-05 and 2.3×10^{37} ergs s^{-1} for 4U 1820-30, a factor of ~ 4 difference. Although it is difficult to disentangle the effects of spectral shape, inclination, and neutral absorption, Figures 7 and 8 suggest that different sources can occupy similar states

and regions of the CCD at very different luminosities.

4U 1915-05 is also similar to 4U 1820-30 in that it exhibits kilohertz QPOs whose behavior depends on position within the CCD (Boirin et al. 2000). As noted above, the frequency of the QPOs increases with S_a , indicating that the inner disk radius is shrinking with increasing accretion rate and that the area of the disk is therefore increasing. Increased soft photon emission from the disk is doubtless contributing to the quenching of the hot corona seen in Figure 5. The RMS amplitude of the QPOs decreases with count rate (although, interestingly, a correlation with S_a is not apparent), and they are not detected at all in the upper banana branch. If the decreasing amplitude is indeed related to accretion rate, this is in agreement with the sonic point beat frequency model of Miller, Lamb, & Psaltis (1998), in which the increasing optical depth of the accretion flow at higher accretion rates inhibits the radiation drag which creates the QPOs in the first place. Twin kilohertz QPOs are detected only in a narrow range of S_a , which corresponds to the “vertex” in the CCD of Figure 2. This is also the range in S_a in which the source makes its rapid transition from the *RXTE* low state (Figure 5) to the high state. In the sonic point model, the second QPO is produced when a portion of the gas is funneled by the NS magnetic field and produces hot spots that modulate the radiation drag at the NS spin frequency. There is no obvious relation to the cutoff energy in this model; perhaps the inner disk reaches a region where the magnetic field is strong enough to produce this funneling at an S_a that just happens also to produce a BB flux strong enough to quench the corona.

6. Conclusions

We have observed 4U 1915-05 in the lower and upper banana states with *RXTE* and find that they correspond to the low/intermediate and high/very soft states defined by Barret et al. (1996) from *Ginga* data (Yoshida 1993). The CPL + BB model provides a good fit to the data, and all spectral parameters show strong correlations with both the 2–50 keV luminosity and the accretion rate parameterized by S_a . The BB temperature kT_{BB} is the most strongly correlated with S_a , and so this component is primarily responsible for driving the accretion-related spectral changes. Spectral parameters are not as well constrained using the CompTT + BB model, and models involving a DBB component do not give realistic fits. Our results are consistent with a geometry in which the soft component arises from an optically thick boundary layer and the hard component from an extended Comptonizing corona. 4U 1915-05 was observed in similar states as was 4U 1820-30 (Bloser et al. 2000), but the states correspond to different values of the total luminosity in the two systems. The CPL component is more prominent in 4U 1915-05 than in 4U 1820-30, as expected for a dimmer source, and this is consistent with differences in the two sources’ color-color diagrams.

We wish to thank A. P. Smale and J. H. Swank for early discussions of the data. This paper had made use of quick-look results provided by the ASM/*RXTE* team. This work was supported

in part by NASA grant NAG5-3298. PFB acknowledges partial support from NASA GSRP grant NGT5-50020.

REFERENCES

- Arnaud, K. A. 1996, in ASP Conf. Ser. 101, *Astronomical Data Analysis Software and Systems V*, ed. J. H. Jacoby & J. Barnes (San Francisco: ASP), 17
- Barret, D., Grindlay, J. E., Harrus, I. M., & Olive, J. F. 1999, *A&A*, 341, 789
- Barret, D., Grindlay, J. E., Strickman, M., & Vedrenne, G. 1996, *A&AS*, 120, 269
- Barret, D., Olive, J. F., Boirin, L., Done, C., Skinner, G. K., & Grindlay, J. E. 2000, *ApJ*, 533, 329
- Barret, D. & Vedrenne, G. 1994, *ApJS*, 92, 505
- Bloser, P. F., et al. 1996, *A&AS*, 120, 275
- Bloser, P. F., Grindlay, J. E., Kaaret, P., Zhang, W., Smale, A. P., & Barret, D. 2000, *ApJ*, in press
- Boella, G., Butler, R. C., Perola, G. C., et al. 1997, *A&AS* 122, 299
- Boirin, L., Barret, D., Olive, J. F., Grindlay, J. E., & Bloser, P. F. 2000, *A&A*, in press
- Bradt, H. V., Rothschild, R. E., & Swank, J. H. 1993, *A&AS*, 97, 355
- Callanan, P. J., Grindlay, J. E., & Cool, A. M. 1995, *PASJ*, 47, 153
- Chou, Y., Bloser, P. F., & Grindlay, J. E. 2000, in preparation
- Church, M. J., et al. 1997, *ApJ*, 491, 388
- Church, M. J., & Balucińska-Church, M. 2000, *ApJ*, submitted
- Church, M. J., Balucińska-Church, M., Dotani, T., & Asai, K. 1998, *ApJ*, 504, 516
- Church, M. J., Parmar, A. N., Balucińska-Church, M., Oosterbroek, T., Dal Fiume, D., & Orlandini, M. 1998, *A&A*, 338, 556
- Ebisawa, K., et al. 1994, *PASJ*, 46, 375
- Grindlay, J. E., Bailyn, C. D., Cohn, H., Lugger, P. M., Thorstensen, J. R., & Wegner, G. 1988, *ApJ*, 334, L25
- Guainazzi, M., Parmar, A. N., Segreto, A., Stella, L., Dal Fiume, D., & Oosterbroek, T. 1998, *A&A*, 339, 802
- Hasinger, G., & van der Klis, M. 1989, *A&A*, 225, 79
- In 't Zand, J. J. M., et al. 1999, 345, 100
- Ko, Y., Mukai, K., Smale, A. P., & White, N. E. 1999, *ApJ*, 520, 292
- Levine, A. M., Bradt, H., Cui, W., Jernigan, J. G., Morgan, E. H., Remillard, R., Shirey, R. E., & Smith, D. A. 1996, *ApJ*, 469, 33

- Méndez, M., van der Klis, M., Ford, E. C., Wijnands, R., & van Paradijs, J. 1999, *ApJ*, 511, L49
- Miller, M. C., Lamb, F. K., & Psaltis, D. 1998, *ApJ*, 508, 791
- Mitsuda, K., Inoue, H., Koyama, K, et al. 1984, *PASJ*, 36, 741
- Morley, R., Church, M. J., Smale, A. P., & Balucińska-Church, M. 1999, *MNRAS*, 302, 593
- Nelson, L. A., Rappaport, S. A., & Joss, P. C. 1986, *ApJ*, 304, 231
- Olive, J. F., Barret, D., Boirin, L., & Grindlay, J. E. 1999, *Adv. Space Res.*, in press
- Piraino, S., Santangelo, A., Ford, E. C., & Kaaret, P. 1999a, to appear in *Proc. 19th Texas Symp. in Paris*
- Piraino, S., Santangelo, A., Ford, E. C., & Kaaret, P. 1999b, *A&A*, 349, L77
- Priedhorsky, W., & Terrell, J. 1984a, *ApJ*, 280, 661
- Priedhorsky, W., & Terrell, J. 1984b, *ApJ*, 284, L17
- Rothschild, R. E., et al. 1998, *ApJ*, 496, 538
- Shimura, T., & Takahara, F. 1995, *ApJ*, 445, 780
- Smale, A. P., & Lochner, J. C. 1992, *ApJ*, 395, 582
- Smale, A. P., Mason, K. O, White, N. E., & Manfred, G. 1988, *MNRAS*, 232, 647
- Sobczak, G. J., McClintock, J. E., Remillard, R., Bailyn, C. D., & Orosz, J. A. 1999, *ApJ*, 520, 776
- Stark, A. A., et al. 1992, *ApJS*, 79, 77
- Sunyaev, R. A., & Shakura, N. I. 1986, *Sov. Ast. Lett.*, 12, 117
- Tavani, M. & Barret, D. 1997, in eds. C. Dermer, M. Strickman, & J. Kurfess, *Proc. of the 4th Compton Symp., AIP Conf. Proc.* 410, 75
- Titarchuk, L. 1994, *ApJ*, 434, 570
- Walter, F. M., et al. 1982, *ApJ*, 253, L67
- White, N. E., Stella, L., & Parmar, A. N. 1988, *ApJ*, 324, 363
- White, N. E., & Swank, J. H. 1982, *ApJ*, 253, L61
- Wilms, J., Nowak, M. A., Dove, J. B., Fender, R. P., & di Matteo, T. 1999, *ApJ*, 522, 460
- Yoshida, K. 1993, PhD Thesis, University of Tokyo

Fig. 1.— *RXTE*/ASM light curve of 4U 1915-05 (2–12 keV) from 1996 March – October (MJD 50150 = 1996 March 7). Each point represents a 1-day average. Pointed PCA/HEXTE observation times are marked with vertical lines.

Fig. 2.— Color-color diagram of 4U 1915-05. Each point represents one of the 70 data segments from Boirin et al. (1999), which have typical lengths of 1200 s. The soft and hard colors are defined as the ratio of background-subtracted count rates in the bands 3.5–6.4 keV and 2.0–3.5 keV, and 9.7–16.0 keV and 6.4–9.7 keV, respectively. Filled symbols indicate data from Epoch 3, open symbols data from Epoch 1. The Epoch 1 points may be positioned incorrectly, due to difficulties in matching energy bands between the two gain epochs. The position within the diagram is parameterized by the variable S_a , the distance along the line.

Fig. 3.— Representative PCA (PCU 0) and HEXTE (cluster B) spectra of 4U 1915-05. On 1996 March 13 the source was in a high state. On 1996 August 16 the source was in the low state and is detected with HEXTE up to 50 keV. The hardening of the spectrum with decreasing luminosity is clear.

Fig. 4.— Examples of 4U 1915-05 spectra fit with the CPL + BB model. The top panel shows the raw count rate spectrum with the fitted model folded through the instruments’ responses, the middle panel shows the residuals of the fit, and the bottom panel shows the unfolded spectrum with the individual model components. The dotted line is the blackbody, the dashed line is the CPL model, and the dash-dot line is the gaussian line (right panel only). On the left is the low state spectrum of 1996 August 16, and on the right is the high state spectrum of 1996 March 13.

Fig. 5.— Variation of spectral parameters for the CPL + BB model with accretion rate, parameterized by S_a . Here kT_{BB} = blackbody temperature, R_{BB} = blackbody radius, α = power law photon index, and E_c = power law cut-off energy. Error bars are 1σ for one interesting parameter. The point with the highest S_a is Epoch 1 data, and this S_a value has been rescaled relative to the others according to total flux.

Fig. 6.— Variation of spectral parameters for the CompTT + BB model with accretion rate, parameterized by S_a . Only the brightest eight spectra could be fit with this model, as the faintest three lacked a discernible cutoff. Here τ = Comptonization optical depth and kT_e = Comptonizing electron temperature. The point with the highest S_a is Epoch 1 data, and this S_a value has been rescaled relative to the others according to total flux.

Fig. 7.— Comparison of fitted parameters for the CPL + BB model for 4U 1915-05 (this paper; assumed distance = 9.3 kpc) and 4U 1820-30 (Bloser et al. 1999; assumed distance = 6.4 kpc). The behavior of the power law component is qualitatively similar but quantitatively different in the two sources in that the rapid transition from a low hard state to a high soft state takes place at very different total luminosities. The behavior of the blackbody component is more quantitatively consistent in the sense that kT_{BB} increases with luminosity until it reaches ~ 2.6 keV.

Fig. 8.— Comparison of the color-color diagrams of 4U 1915-05 (open symbols) and 4U 1820-30 (closed symbols; Bloser et al. 1999). The S_a tracks are included for clarity. Except for the 4U 1820-30 island state, the hard color in 4U 1915-05 is always greater than that in 4U 1820-30, though both sources cover the same range in soft color.

Table 1. Previous Spectral Results on 4U 1915-05

Experiment	Year	Model ^a	N_H (10^{21} cm ⁻²)	Luminosity ^b (10^{37} ergs s ⁻¹)
<i>OSO-8</i>	78	PL ($\alpha = 1.6$ – 1.7)
<i>Einstein</i> (MPC+SSS)	79	BR ($kT_{BR} = 12$ keV)	3.0	1.0–1.3 (0.5–60 keV)
<i>EXOSAT</i>	83 & 85	PL ($\alpha = 1.8$)	2.1	0.66 (0.1–15 keV)
<i>Ginga</i> (high)	90	CPL ($\alpha = 1.0$, $E_c \sim 8$ – 10 keV)	1.3	1.2 (1–37 keV)
<i>Ginga</i> (intermediate)	87 & 88	CPL ($\alpha = 1.7$, $E_c \gtrsim 50$ keV)	0.2	0.6–0.7
<i>Ginga</i> (low)	88	CPL ($\alpha = 1.5$, $E_c \sim 25$ keV)	0.6	0.3
<i>CGRO</i> (OSSE)	95	< 0.017 (50–98 keV)
<i>CGRO</i> (BATSE)	91–95	< 0.63 (20–100 keV)
<i>ASCA</i>	93	BB+PL ($kT_{BB} = 2.14$ keV, $\alpha = 2.42$)	4.75	0.29 (1–10 keV)
<i>ROSAT</i> (PSPC)	92	BB+PL ($kT_{BB} = 1.95$ keV, $\alpha = 2.32$)	3.9	... (0.1–2 keV)
<i>BeppoSAX</i>	97	BB+CPL ($kT_{BB} = 1.62$ keV, $\alpha = 1.61$, $E_c = 80 \pm 10$ keV)	3.2	0.25 (1–10 keV)

^aPL = Power Law; BR = Bremsstrahlung; CPL = Cut-off Power Law; BB = Blackbody; α = power law photon index; kT_{BR} = Bremsstrahlung temperature; kT_{BB} = blackbody temperature; E_c = exponential cut-off energy

^bLuminosity assumes a distance of 9.3 kpc

References. — (1) White & Swank 1982; (2) Smale et al. 1988; (3) Yoshida 1993; (4) Barret et al. 1996; (5) Barret et al. 1996; (6) Church et al. 1997; (7) Morley et al. 1999; (8) Church et al. 1998

Table 2. Spectral Fits of 4U 1915-05 with the CPL + BB Model

S_a	Int Time (s)		kT_{BB}^a	R_{BB}^b	α^c	E_c^d	L^e	L_{BB}/L_H^f	χ_ν^2
	PCA	HEXTE	(keV)	(km)		(keV)			
1.09	7755	2509	$1.37^{+0.03}_{-0.02}$	$1.14^{+0.07}_{-0.06}$	$1.80^{+0.02}_{-0.02}$	> 119	0.60	0.12	0.68
1.20	8249	2669	$1.42^{+0.03}_{-0.03}$	$0.90^{+0.07}_{-0.06}$	$1.89^{+0.02}_{-0.02}$	> 115	0.51	0.12	0.79
1.28	7361	2485	$1.48^{+0.03}_{-0.03}$	$0.92^{+0.07}_{-0.06}$	$1.95^{+0.02}_{-0.02}$	> 104	0.57	0.12	0.81
1.36	14030	4630	$1.51^{+0.06}_{-0.05}$	$0.84^{+0.06}_{-0.06}$	$1.85^{+0.09}_{-0.08}$	$31.25^{+19.16}_{-7.48}$	0.54	0.11	0.69
1.44	20948	6450	$1.63^{+0.03}_{-0.04}$	$0.84^{+0.04}_{-0.04}$	$1.95^{+0.08}_{-0.08}$	$34.14^{+18.51}_{-8.88}$	0.62	0.14	0.55
1.52	7396	2383	$1.79^{+0.05}_{-0.06}$	$0.78^{+0.08}_{-0.09}$	$1.64^{+0.12}_{-0.12}$	$12.65^{+3.12}_{-2.11}$	0.66	0.13	0.87
1.65	1856	634	$2.01^{+0.07}_{-0.06}$	$0.99^{+0.12}_{-0.10}$	$1.71^{+0.20}_{-0.16}$	$13.17^{+6.91}_{-2.88}$	0.85	0.23	0.76
1.74	2640	874	$2.04^{+0.06}_{-0.05}$	$0.82^{+0.10}_{-0.11}$	$1.70^{+0.17}_{-0.16}$	$14.31^{+6.61}_{-3.30}$	0.91	0.24	0.68
1.85	2829	951	$2.27^{+0.11}_{-0.09}$	$0.74^{+0.12}_{-0.09}$	$1.45^{+0.18}_{-0.13}$	$8.90^{+2.56}_{-1.35}$	0.95	0.25	0.71
1.95	3030	961	$2.24^{+0.13}_{-0.07}$	$0.78^{+0.09}_{-0.11}$	$1.37^{+0.13}_{-0.17}$	$8.92^{+1.69}_{-1.56}$	1.00	0.24	0.79
2.79 ^g	2802	928	$2.46^{+0.39}_{-0.09}$	$0.65^{+0.08}_{-0.04}$	$1.30^{+0.11}_{-0.10}$	$9.08^{+1.39}_{-0.69}$	1.44	0.23	0.68

^aBlackbody temperature

^bBlackbody radius

^cCut-off power law photon index

^dCut-off power law cut-off energy or lower limit

^eTotal luminosity, $\times 10^{37}$ ergs s⁻¹, for a distance of 9.3 kpc, 2–50 keV

^fRatio of blackbody flux to power law flux, 2–50 keV

^gIncluded gaussian line; $E_l = 6.14^{+0.18}_{-1.07}$ keV

Note. — For all fits N_H is frozen at 0.2×10^{22} cm⁻². Errors are 1σ for one interesting parameter.

Table 3. Spectral Fits of 4U 1820-30 with the CompTT + BB Model

S_a	kT_{BB} (keV)	R_{BB} (km)	τ^a	kT_e^b (keV)	kT_W^c (keV)	y^d	R_W^e (km)	L	L_{BB}/L_H	χ_ν^2
1.36	$1.49^{+0.08}_{-0.04}$	$0.95^{+0.07}_{-0.10}$	$7.63^{+0.51}_{-1.48}$	$6.80^{+2.77}_{-0.62}$	$0.37^{+0.06}_{-0.09}$	3.10	$20.54^{+7.38}_{-9.94}$	0.52	0.16	0.68
1.44	$1.63^{+0.03}_{-0.06}$	$0.89^{+0.08}_{-0.04}$	$6.40^{+1.16}_{-1.00}$	$8.34^{+2.55}_{-1.87}$	$0.39^{+0.04}_{-0.07}$	2.67	$20.92^{+5.33}_{-8.48}$	0.61	0.19	0.54
1.52	$1.72^{+0.11}_{-0.07}$	$1.01^{+0.04}_{-0.10}$	$8.74^{+0.69}_{-1.80}$	$4.96^{+1.78}_{-0.43}$	$0.46^{+0.04}_{-0.03}$	2.97	$15.13^{+3.50}_{-3.32}$	0.65	0.21	0.84
1.65	$1.93^{+0.07}_{-0.09}$	$1.15^{+0.09}_{-0.08}$	$8.08^{+1.86}_{-3.55}$	$5.34^{+8.39}_{-1.16}$	$0.46^{+0.04}_{-0.06}$	2.73	$16.76^{+10.50}_{-6.89}$	0.84	0.36	0.74
1.74	$2.03^{+0.04}_{-0.07}$	$0.90^{+0.09}_{-0.09}$	$5.78^{+2.71}_{-4.24}$	$8.85^{+67.12}_{-3.67}$	$0.50^{+0.03}_{-0.04}$	2.31	$15.53^{+41.47}_{-8.65}$	0.92	0.43	0.63
1.85	$1.87^{+0.12}_{-0.18}$	$0.91^{+0.10}_{-0.10}$	$12.43^{+1.23}_{-1.53}$	$3.44^{+0.43}_{-0.26}$	$0.39^{+0.06}_{-0.21}$	4.16	$21.81^{+6.74}_{-23.69}$	0.93	0.19	0.67
1.95	$2.03^{+0.12}_{-0.15}$	$1.00^{+0.08}_{-0.08}$	$10.49^{+1.97}_{-3.10}$	$4.09^{+2.11}_{-0.58}$	$0.50^{+0.05}_{-0.05}$	3.52	$13.95^{+4.41}_{-4.28}$	0.99	0.34	0.78
2.79	$1.75^{+0.13}_{-0.14}$	$1.00^{+0.11}_{-0.08}$	$13.46^{+0.74}_{-0.89}$	$3.53^{+0.22}_{-0.15}$	$0.34^{+0.07}_{-0.34}$	5.01	$33.71^{+14.74}_{-67.25}$	1.41	0.15	0.71

^aComptonizing cloud optical depth

^bComptonizing electron temperature

^cTemperature of seed photons (assumed to follow a Wien law)

^dComptonization parameter $y = 4kT_e\tau^2/m_e c^2$

^eEquivalent Wien radius of seed photons (see text)

Note. — For all fits N_H is frozen at $0.2 \times 10^{22} \text{ cm}^{-2}$. Errors are 1σ for one interesting parameter.

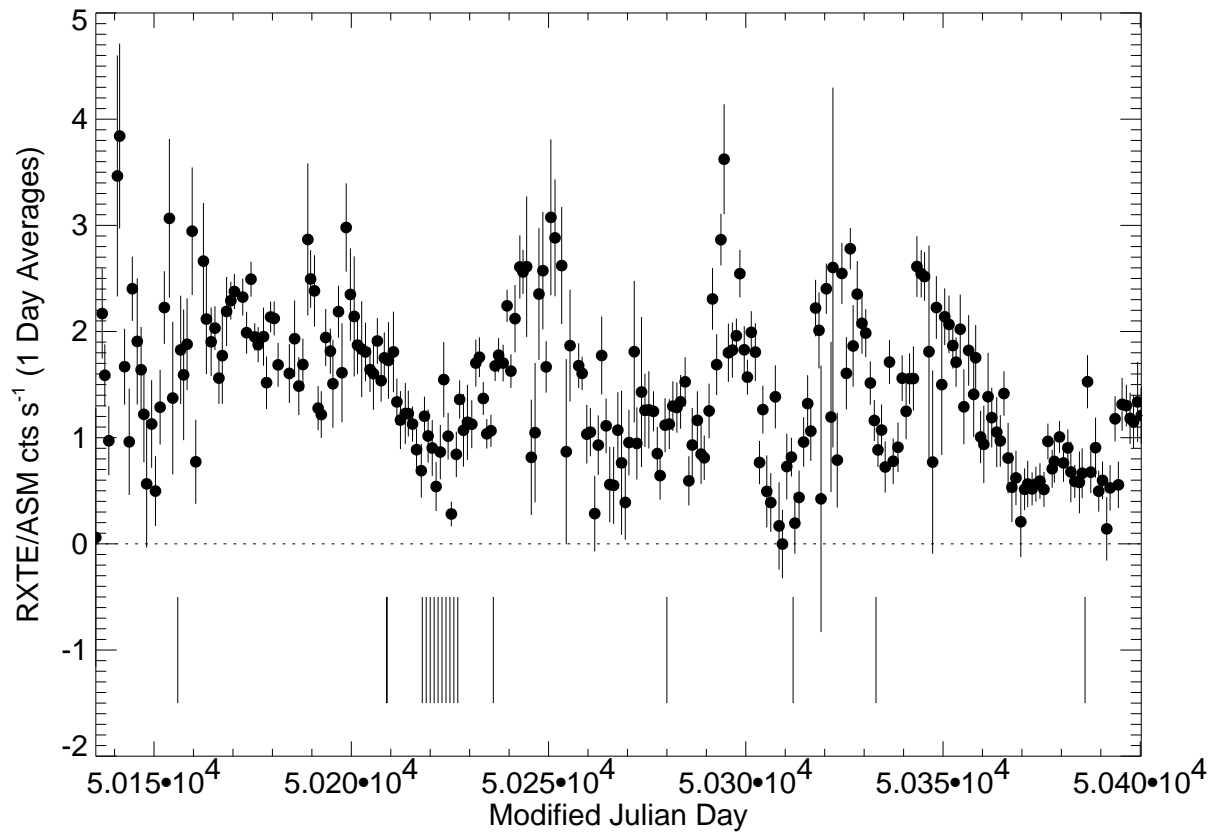


Fig. 1.—

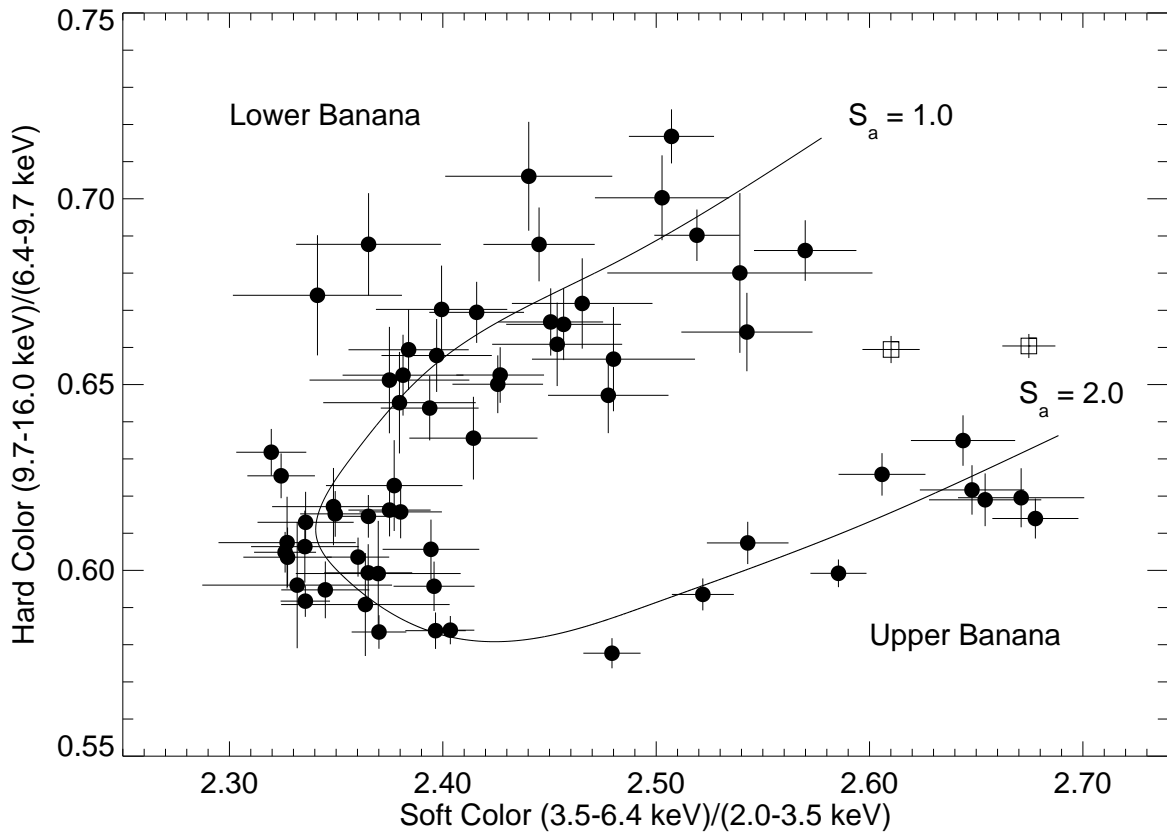


Fig. 2.—

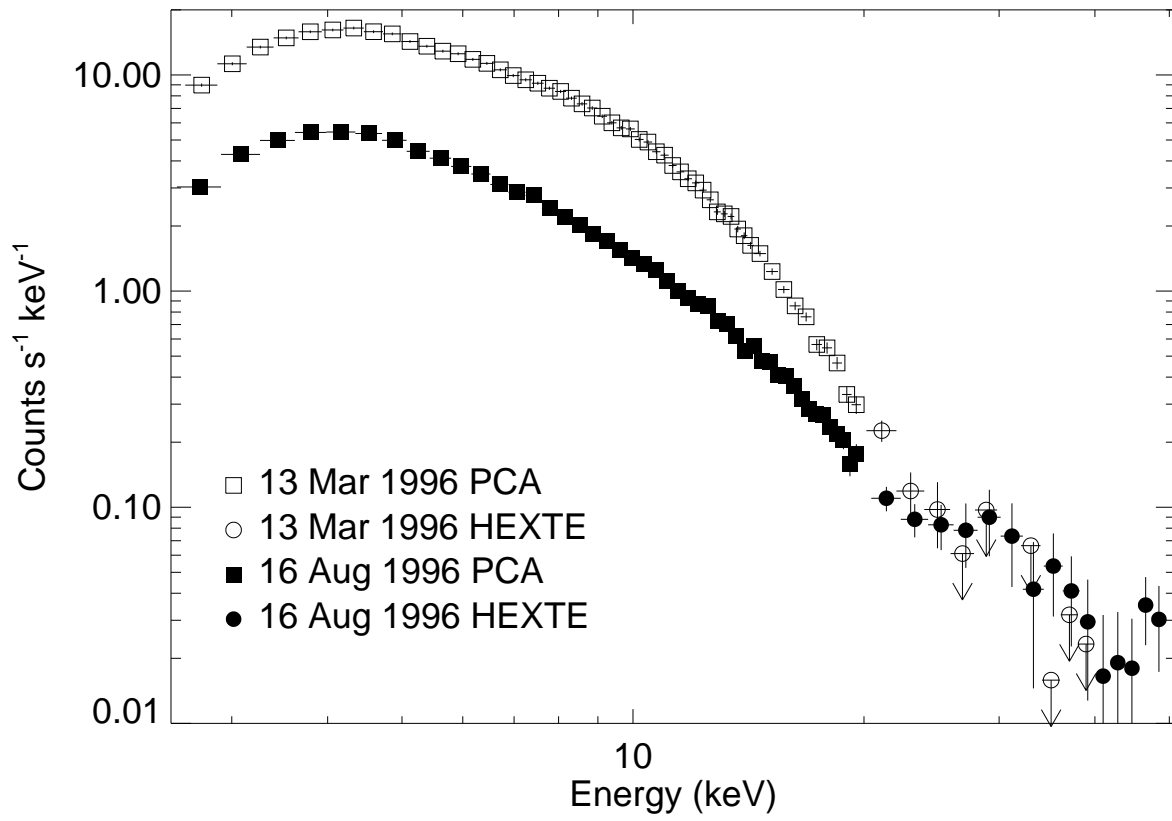


Fig. 3.—

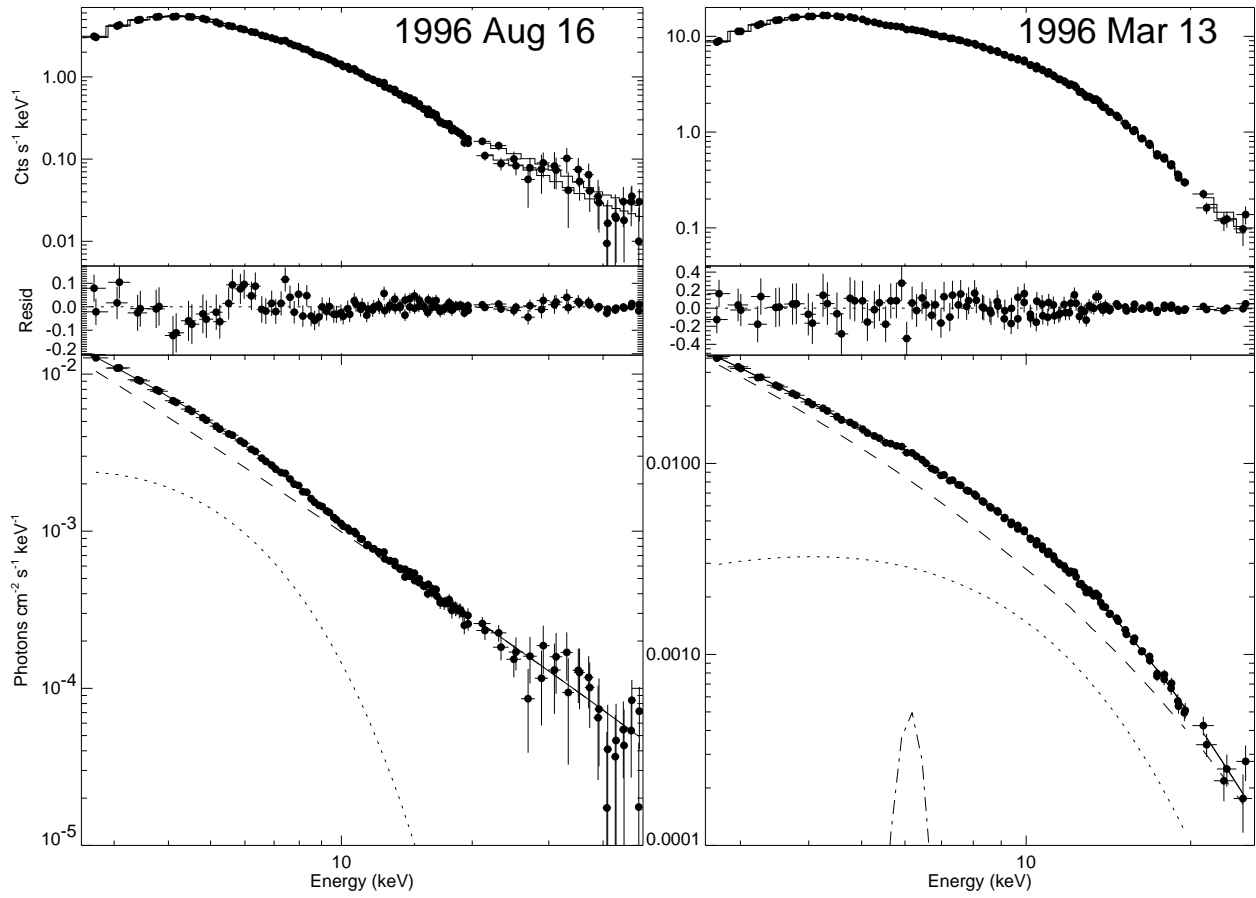


Fig. 4.—

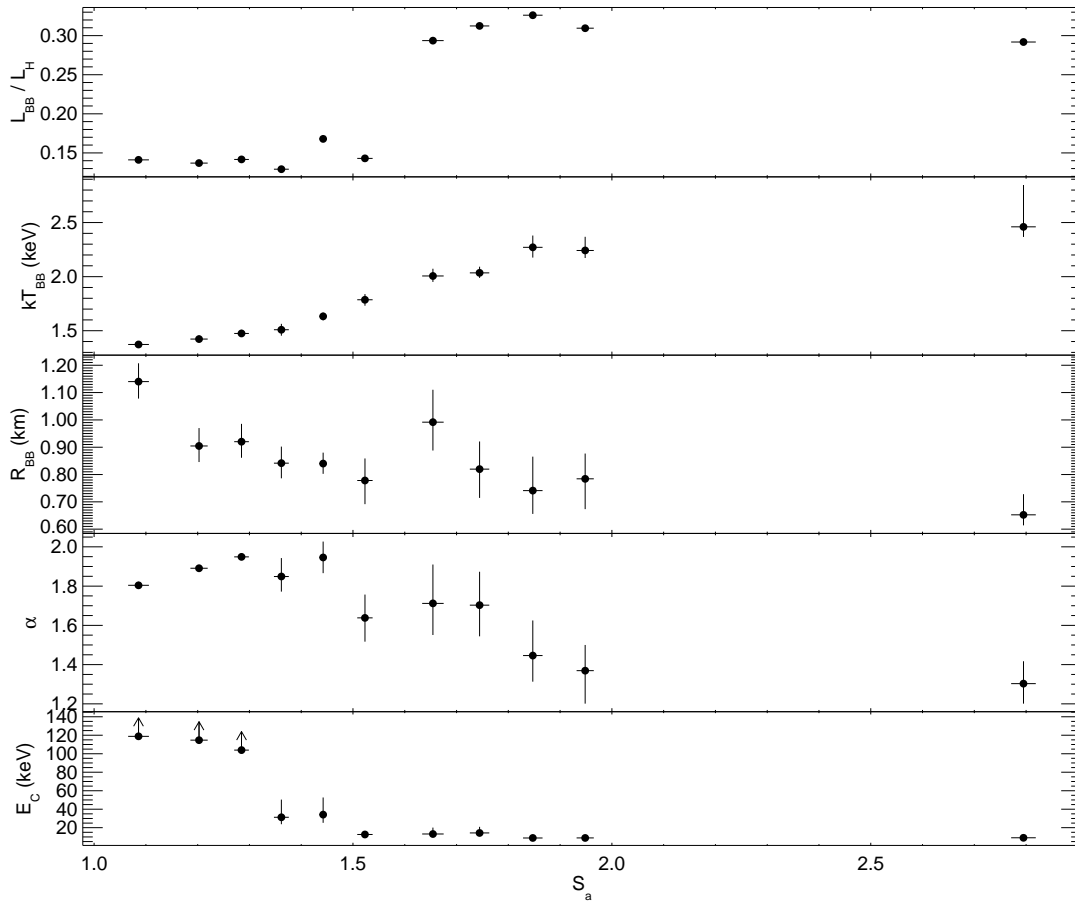


Fig. 5.—

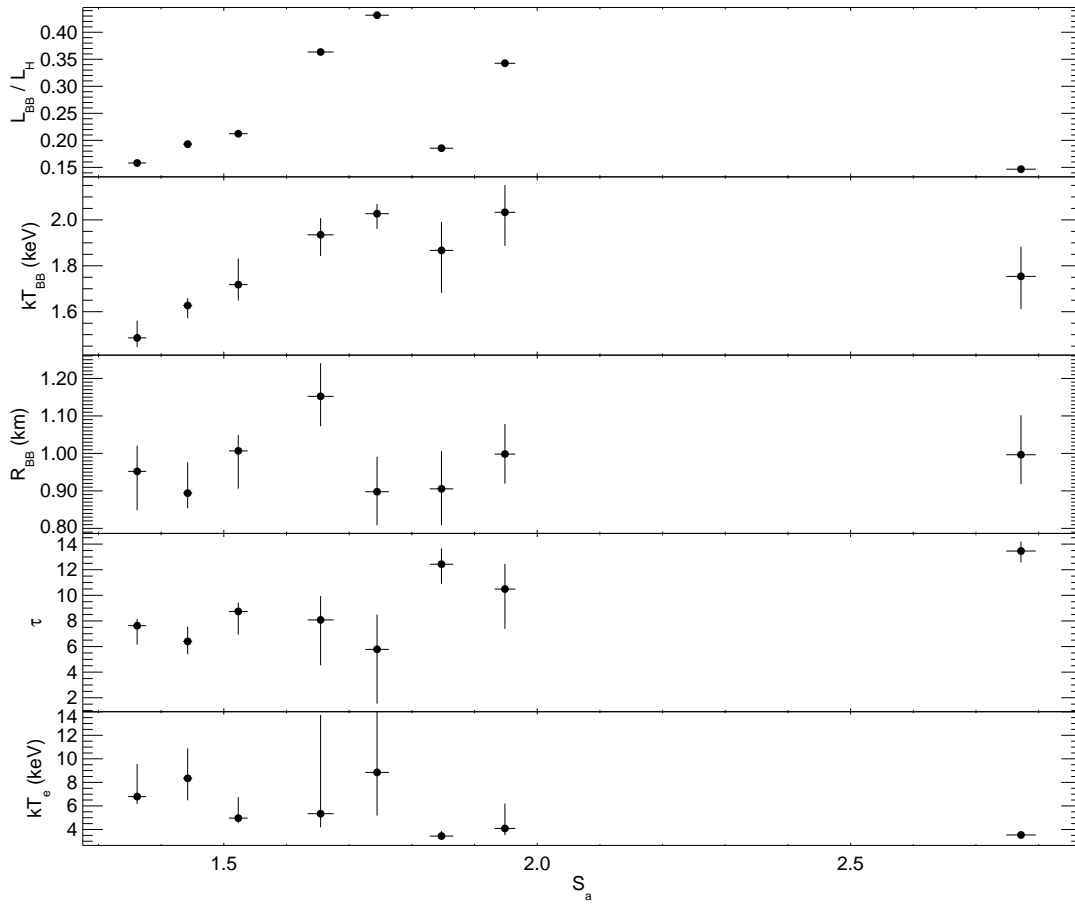


Fig. 6.—

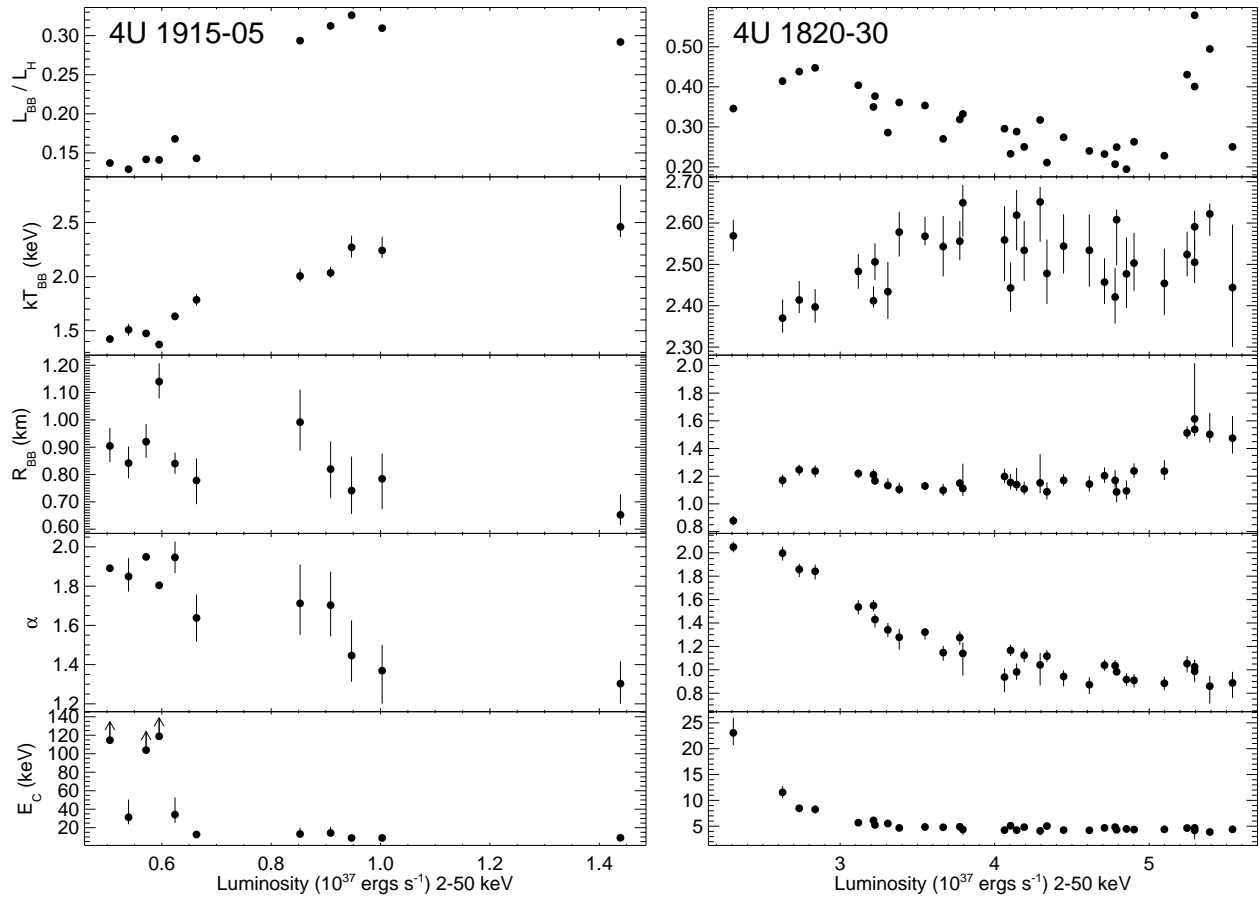


Fig. 7.—

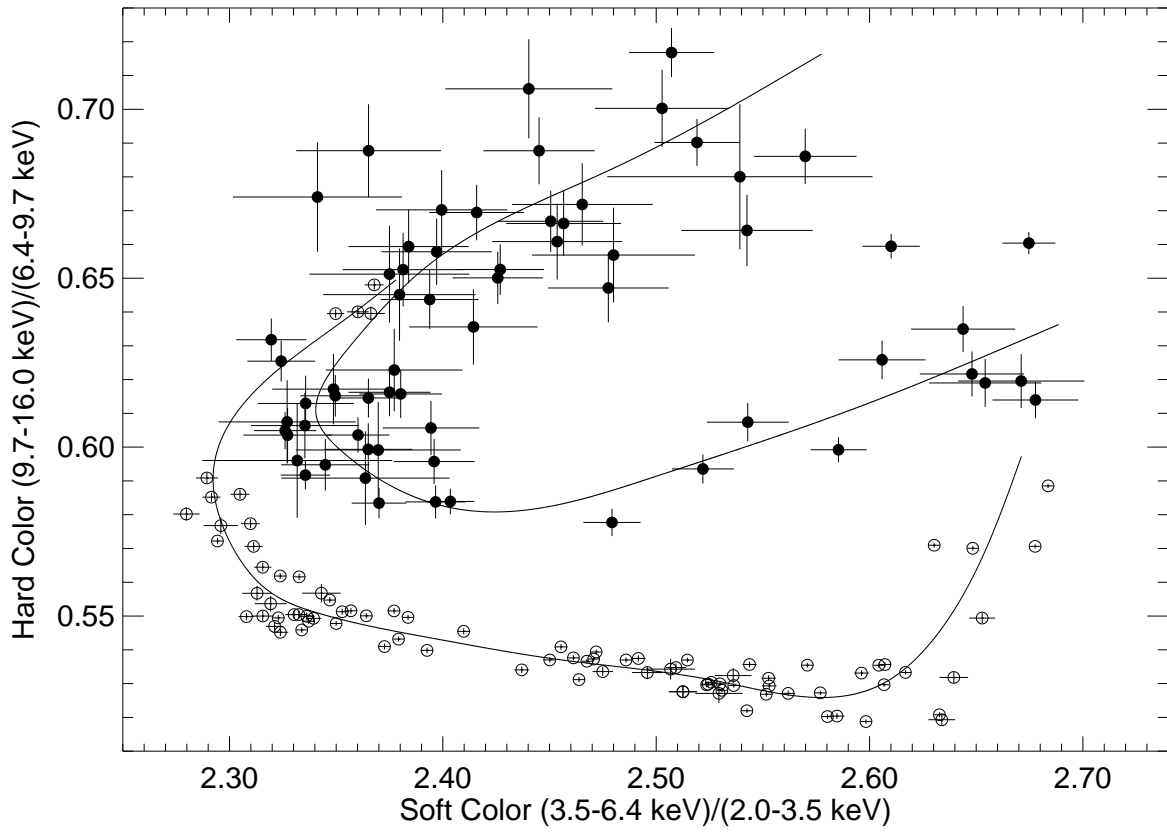


Fig. 8.—